Control and analysis of single-determinant electron dynamics

Raghunathan Ramakrishnan* and Mathias Nest
Theoretische Chemie, TU München, Lichtenbergstrasse 4, 85747 Garching, Germany
(Received 14 March 2012; published 3 May 2012)

Methods which use time-dependent orbitals for the description of quantum dynamics of electrons, like (multiconfiguration) time-dependent Hartree-Fock or time-dependent density-functional theory, produce an effectively time-dependent electronic structure. This effect is strongest if only a single determinant represents the system. Focusing on this case, we show how features of the time-dependent electronic structure show up in optimized laser pulses used for the coherent control task of a population inversion.

DOI: 10.1103/PhysRevA.85.054501 PACS number(s): 31.15.B−, 03.65.Ge, 71.10.Li

Over the last decade many electronic structure methods have been extended from the time-independent to the time-dependent realm, opening the way to first-principles quantum dynamics of many-electron systems. This has been of special interest for both physicists and chemists: for physicists, because attosecond physics became experimentally feasible, and for chemists, because the making and breaking of bonds, made of valence electrons, is at the basis of chemistry. The properties of these time-dependent methods are by now well known: If one looks at correlated wave-function-based methods like the time-dependent configuration-interaction (TDCI) [1,2] and multiconfiguration time-dependent Hartree-Fock (MCTDHF) [3–5] methods, then we find that only up to around 100 electrons can be treated by the former and around 10 electrons by the latter method. Given that a small molecule like benzene already has 42 electrons, there is an obvious demand for faster or more efficient methods. Two methods come here to mind: the time-dependent Hartree-Fock (TDHF) method [6] and the time-dependent density functional theory in the Kohn-Sham formalism (TDKS) [7–9]. Both methods are very similar, because they propagate only a small set of orbitals, and TDHF can actually also be seen as a version of TDKS with exact exchange and no correlation functional (EXX) [10]. However, these methods also have their drawbacks: TDKS in the adiabatic approximation lacks a memory kernel, while the TDHF method lacks correlation. Also, it is very difficult to combine both with coherent control, although some progress has been made recently [11,12]. The reason is twofold: First, the equations of motion (EOM) of the spin orbitals ψ are nonlinear,

$$\dot{\psi}_j = -ih_{\text{eff}}[\rho(t)]\psi_j, \tag{1}$$

(we are using atomic units throughout) because the effective single-particle Hamiltonian depends on the density, which in turn depends on the orbitals. And second, methods involving time-dependent orbitals produce an effectively time-dependent electronic structure [13,14]. As a consequence, simple, analytical pulses, e.g., π pulses for population inversion, become insufficient [15]. It is the purpose of this Brief Report to demonstrate the connection between the time-dependent electronic structure and features of a control laser pulse.

The system which we employ to study the electron dynamics is the one-dimensional Hooke atom, which has been widely used as a benchmark system in time-dependent density functional theory (TDDFT) [16–18]. The spring constant has been chosen to be 0.1 a.u., and the electron-electron repulsion is screened according to

$$V_{ee}(r_1,r_2) = \frac{1}{\sqrt{(r_1-r_2)^2+1}}. \tag{2}$$

The time-dependent spatial orbitals $\varphi_j(r,t)$ are represented in the basis of the harmonic oscillator eigenstates $|n\rangle$

$$\varphi_j(r,t) = \sum_{n=0}^{M-1} c_{jn}(t)|n\rangle, \quad j = 1,\ldots,M, \tag{3}$$

with molecular orbital (MO) coefficients $\{c_{jn}\}$. Time-dependent spin orbitals, $\psi_j(x,t)$, are then obtained by multiplication with either spin up or spin down, and x is a combined position and spin variable. For a one-dimensional, closed-shell two-electron system, the time-dependent Hartree-Fock or Kohn-Sham wave function is given by

$$|\Psi(x_1,x_2,t)\rangle = |\psi(x_1,t)\overline{\psi}(x_2,t)\rangle. \tag{4}$$

As we are aiming to achieve a state-to-state transition in this system, it is necessary to identify excited states. Several procedures exist to define these in the context of the TDHF method and TDDFT. From a quantum-dynamical perspective the most important requirement for these states is that they should be stationary states [19]. In other words, if we start a (field-free) propagation in one of these states, the modulus of the autocorrelation function should be time independent and equal to 1. For the small system considered in this Brief Report these stationary states can be found by a simple scan of all possible combinations of MO coefficients, followed by an ultrashort time propagation. The $\{c_{jn}\}$ thus found are accurate up to at least 10^{-8}.

For $M = 2$, the two stationary values of c_{10} were found to be 1.0 and 0.0, implying no mixing between the basis functions. For $M = 3$ there are three stationary states corresponding to $\{c_{10} = 0.98836287, c_{11} = 0.0, c_{12} = 0.15211455\}$, $\{c_{20} = 0.0, c_{21} = 1.0, c_{22} = 0.0\}$, and $\{c_{30} = 0.00925970, c_{31} = 0.0, c_{32} = 0.99995713\}$. Here it is interesting to note that the stationary orbitals φ_1 and φ_3 hence obtained are not orthogonal, and they represent two coplanar vectors forming an angle of 80.72°. We denote the corresponding Slater determinants of the three-level system as $|1\overline{1}\rangle$, $|2\overline{2}\rangle$, and $|3\overline{3}\rangle$, where the ground and the second excited state are

*rama@mytum.de

nonorthogonal:

$$\langle 1\bar{1}|3\bar{3}\rangle \approx 0.026. \tag{5}$$

This is a general feature of the nonlinear equations of motion, which holds for all cases $M \geqslant 3$. By increasing the variational space to up to four and five basis functions, we optimized the stationary states, where for $M = 5$ the first and third excited states are of ungerade symmetry while the other states are of gerade spatial symmetry. As a general trend, we note that any two states of different spatial symmetry are orthogonal to each other.

Such a search for stationary states is of course only possible for small model systems, as the one used here. For real many-electron systems it is necessary to derive electronic structure information from the time-dependent wave function. One tool that is often used in this context is the autocorrelation function (ACF) and its Fourier transform. But here we encounter two problems: First, if TDKS equations of motion are used, the wave function is usually not a good state vector, which makes the interpretation of the overlap of wave functions at different times difficult. And second, because of the nonorthogonality of the stationary states, it is questionable to interpret the modulus squared of the autocorrelation as the probability of being in the ground state, although this is sometimes done.

Another often-used tool is the Fourier transform of the oscillating dipole moment. In contrast to the ACF, this is a good quantity even in the context of TDKS. However, also this quantity has to be used with care. For example, for the $M = 2$ system the energy difference between the ground and excited states is 0.492 a.u. If we now prepare a wave packet at time $t = 0$ as an orbital that is a superposition of the stationary orbitals

$$|\varphi(t=0)\rangle = \alpha|\varphi_1\rangle + \sqrt{1-\alpha^2}|\varphi_2\rangle, \tag{6}$$

the Fourier transform of the oscillating dipole moment should have a peak at ΔE. However, this is not the case, as can be seen in Fig. 1(a). There the peak position is shown for various values of α, with the excitation energy of the wave packet as

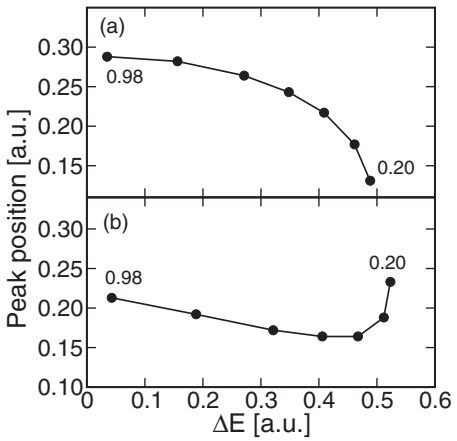

FIG. 1. Peak position of the Fourier transform of the oscillating dipole moment. The numbers next to the dots give the value of α and the horizontal axis is the excitation energy of the wave packet. The initial state is given by Eq. (6). (a) A wave packet with $M = 2$; (b) a wave packet with with $M = 3$.

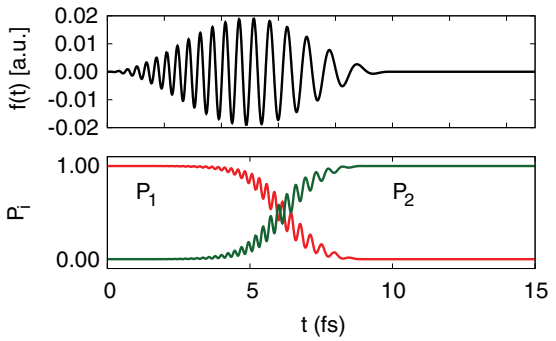

FIG. 2. (Color online) Top: chirped laser pulse, with parameters $f_0 = 0.019031$ a.u., $\omega_0 = 0.499844$ a.u., and $\omega_1 = -0.000508$ a.u. and duration 10 fs. Bottom: population inversion due to the laser pulse.

the horizontal axis. The peak is for no wave packet close to the energy difference of the stationary states. This is not really surprising, because neither state is represented very well during the propagation. Moreover, the result depends on the value of α. Therefore, if energy is continuously pumped into the system, one has to expect a time-dependent effective electronic structure, with time-dependent resonance conditions.

To show this, we demonstrate a state-to-state transition, for $M = 2$, using a chirped laser pulse with the functional form

$$f(t) = f_0 \sin^2\left[\frac{\pi}{2\sigma}t\right]\sin[(\omega_0 + \omega_1 t)t], \quad t < 2\sigma. \tag{7}$$

Here, f_0 is the field strength, ω_0 the carrier frequency, and ω_1 a chirp parameter. The pulse duration $2\sigma = 10$ fs is fixed, and all other parameters are optimized. For the optimization problem we used the bisection global optimization scheme [20], after choosing a suitable range of variables from a coarse scan of the parameters. Figure 2 shows the pulse (for parameters see Table I) and the populations during the $|1\bar{1}\rangle \rightarrow |2\bar{2}\rangle$ transition. The instantaneous population of a stationary state is computed as

$$P_n(t) = |\langle\psi_n|\psi(t)\rangle|^2. \tag{8}$$

The negativity of the optimal chirp ($\omega_1 = -0.000508$ a.u.) agrees with the redshift of the peak in Fig. 1(a): As more energy is pumped to the system, the energy gap between the two systems seems to become smaller.

The laser parameters given above are the best that can be found in the interval that we scanned, but other parameters

TABLE I. Optimal control parameters (in a.u.) for the $|1\bar{1}\rangle \rightarrow |2\bar{2}\rangle$ population inversion in the case of two, three, four, and five basis functions. Also given is the fitness, i.e., one minus the average overlap of the time-dependent orbital and the target orbital for a period of 5 fs after the end of the pulse.

M	f_0	ω_0	ω_1	Fitness
2	0.019031	0.499844	−0.000508	0.00000
3	0.102063	0.234844	0.000043	0.00672
4	0.103125	0.249375	0.000030	0.02095
5	0.101953	0.249219	0.000037	0.08465

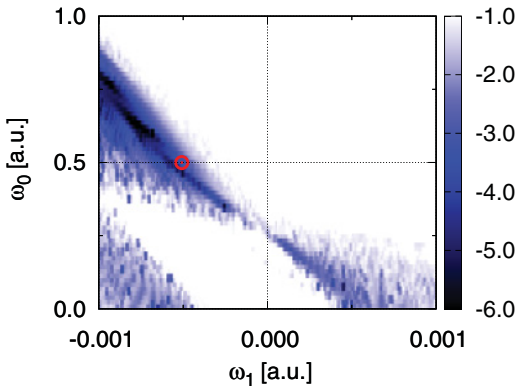

FIG. 3. (Color online) Fitness scan for laser parameters ω_0 and ω_1, with optimized fluence at each point (logarithmic scale). A fitness of zero corresponds to an optimal pulse.

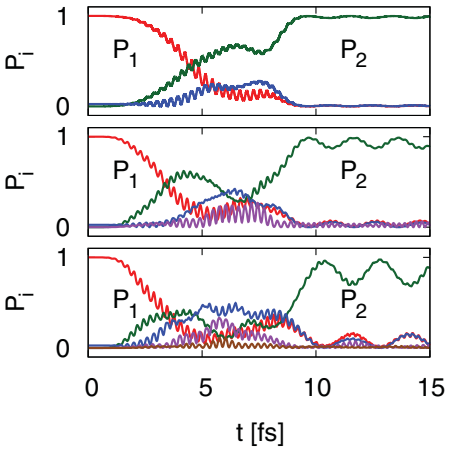

FIG. 4. (Color online) Time-dependent populations of the (top) three-, (middle) four-, and (bottom) five-level systems; see Table I for pulse parameters. The simple parametrized laser pulse given in Eq. (7) is not able to achieve the transition $|1\bar{1}\rangle \rightarrow |2\bar{2}\rangle$ for $M > 3$. Also visible, the populations of the final states are not constant when the laser pulse is switched off.

are possible which still perform the control task relatively well. If we define a fitness function as the average of $1 - |\langle\psi_{\text{target}}|\psi(t)\rangle|^2$ during the field-free evolution of 5 fs after the end of the pulse, we find multiple local minima. Figure 3 shows the logarithm of the fitness function for a scan over intervals of ω_0 and ω_1, where at each point the field strength is optimized. The global optimum of the fitness in that area is marked with a red circle. Other "good" pulse parameters lie along a valley with a stronger chirp with increasing carrier frequency. All these pulses have in common that they have a significant intensity around a frequency of 0.4 a.u., during the middle or end of their duration, which is somewhat less than the vertical excitation energy of 0.492 a.u. The rugged character of the control surface makes it more difficult to identify the global minimum, which could not be found by simple steepest-descent methods. This ruggedness is only partially due to the optimization of the field strength for each pair (ω_0, ω_1). Even straight two-dimensional (2D) cuts through the three-dimensional (3D) parameter space show multiple minima, although not as strongly as in Fig. 3.

Up to here, we have only discussed calculations with $M = 2$ basis functions. If we increase this number, it becomes increasingly more difficult to perform the control task. The top panel of Fig. 4 shows the population dynamics for three basis functions ($M = 3,4,5$). Here, the population inversion is still almost complete. But if four or five basis functions are used, which is still far from a full basis-set limit, we see that a full inversion becomes impossible. The last statement has to be understood in the sense that we only optimized the parametrized laser pulse given by Eq. (7). With a more flexible pulse, one can expect a somewhat better performance. The failure to perform the control task is mainly due to the increased state space over which the populations become distributed. But Fig. 4 shows also something else: For four and five basis functions the populations of the "stationary" states are not constant after the laser pulse has been switched off. This is due to the nonlinearity of the equations of motion, where the Hamiltonian that generates the dynamics depends on the density (matrix). If the density at $t = 10$ fs is not that of a stationary state, then the Hamiltonian itself will be time dependent.

The optimal laser pulse parameters are given in Table I, together with their fitness. Two changes are remarkable when we go from a two-level to a many-level system. First, the carrier frequency ω_0 is decreased by about a factor of 2, while the field strength increases by a factor of about 5. This shows that the preferred mechanism is now a two-photon absorption. The reason for this is that our system is almost harmonic at low energies, so an excitation with the old ($M = 2$) parameters leads to a ladder climbing to higher states. In fact, there is an optimum for the population of the second excited state at $f_0 = 0.017$ a.u., $\omega_0 = 0.507$ a.u., and $\omega_1 = -0.000498$ a.u., which differs only slightly from the corresponding two-level parameters. The near equidistance of the energy levels is a consequence of the Hookean atom model that we used, which will of course only rarely be observed for real molecules. The second change is that the pulse is now blueshifted with a reduction in the chirp parameter by about a factor of 10 to 15. This coincides with a different peak shift, as shown in Fig. 1(b). The change in the peak position is neither strictly positive nor negative, so effectively almost no pulse chirp is necessary.

To conclude, we have shown for a model atomic system that coherent control combined with single-determinant electron dynamics becomes increasingly more complicated when the size of the basis set is increased. If the equations of motion were linear, by the definition of coherent control [21] the probability density can be steered to the desired state using resonance conditions. However, the EOM of TDHF and TDKS methods are nonlinear and lead to an effectively time-dependent electronic structure. We have also shown that it is indeed this phenomenon that is at the heart of the problem, by introducing a chirp into the laser pulse. The chirp follows the electronic structure qualitatively, so the resonance condition is fulfilled better for a longer time. For real atoms and molecules this means that much more complicated laser pulses will be necessary, and that these pulses might not be similar to the one which actually performs the control task in experiment. However, this does not imply

that all observables one might be interested in are necessarily inaccurate, too. Additionally, the quality of the predictions depends on the effective single-particle Hamiltonian. Both the Fock operator and the exchange-correlation potentials were developed for ground-state calculations. It remains to be seen whether Hamiltonians specially adapted to quantum dynamics will perform better.

The authors are grateful for the financial support of the DFG excellence cluster Munich Centre for Advanced Photonics.

[1] T. Klamroth, Phys. Rev. B **68**, 245421 (2003).
[2] P. Krause, T. Klamroth, and P. Saalfrank, J. Chem. Phys. **127**, 034107 (2007).
[3] F. Zanghellini, M. Kitzler, C. Fabian, T. Brabec, and A. Scrinzi, Laser Phys. **13**, 1064 (2003).
[4] F. Remacle, M. Nest, and R. D. Levine, Phys. Rev. Lett. **99**, 183902 (2007).
[5] T. Kato and H. Kono, Chem. Phys. Lett. **392**, 533 (2004).
[6] K. C. Kulander, Phys. Rev. A **36**, 2726 (1987).
[7] E. Runge and E. K. U. Gross, Phys. Rev. Lett. **52**, 997 (1984).
[8] *Time-Dependent Density Functional Theory*, edited by M. A. L. Marques, C. A. Ullrich, F. Nogueira, A. Rubio, K. Burke, and E. K. U. Gross (Springer-Verlag, Heidelberg, 2006).
[9] *Fundamentals of Time-Dependent Density Functional Theory*, edited by M. A. L. Marques, N. T. Maitra, F. M. S. Nogueira, E. K. U. Gross, and A. Rubio (Springer-Verlag, Heidelberg, 2012).
[10] J. I. Fuks, N. Helbig, I. V. Tokatly, and A. Rubio, Phys. Rev. B **84**, 075107 (2011).
[11] A. Castro, J. Werschnik, and E. K. U. Gross, e-print arXiv:1009.2241v1.
[12] M. Mundt and D. J. Tannor, New J. Phys. **11**, 105038 (2009).
[13] R. Padmanaban and M. Nest, Chem. Phys. Lett. **463**, 263 (2008).
[14] S. Raghunathan and M. Nest, J. Chem. Theory Comput. **8**, 806 (2012).
[15] S. Raghunathan and M. Nest, J. Chem. Theory Comput. **7**, 2492 (2011).
[16] N. H. March, J. Chem. Phys. **118**, 6846 (2003).
[17] P. M. W. Gill and D. P. O'Neill, J. Chem. Phys. **122**, 094110 (2005).
[18] M. Thiele and S. Kümmel, Phys. Chem. Chem. Phys. **11**, 4631 (2009).
[19] K. J. H. Giesbertz, K. Pernal, O. V. Gritsenko, and E. J. Baerends, J. Chem. Phys. **130**, 114104 (2009).
[20] G. Wood, in *Encyclopedia of Optimization*, edited by C. A. Floudas and P. M. Pardalos, Vol. 2 (Kluwer, Dordrecht, 2001), pp. 186–189.
[21] H. Rabitz, AIP Conf. Proc. **963**, 249 (2007).